Applied Catalysis B: Environmental 174–175 (2015) 413–420

Contents lists available at ScienceDirect

Applied Catalysis B: Environmental

journal homepage: www.elsevier.com/locate/apcatb

# The effect of active sites' nature on the photo-catalytic performance of Cr-TUD-1 in the oxidation of C1–C3 hydrocarbons

Mohamed S. Hamdy[a,b,*], Guido Mul[b]

[a] Chemistry Department, Faculty of Science, King Khalid University, P.O. Box 9004, Abha 61413, Saudi Arabia
[b] Photocatalytic Synthesis Group (PCS), Faculty of Science and Technology, MESA+ Institute for Nanotechnology, University of Twente, Enschede, The Netherlands

ARTICLE INFO

*Article history:*
Received 16 January 2015
Received in revised form 8 March 2015
Accepted 19 March 2015
Available online 20 March 2015

*Keywords:*
Cr-TUD-1
Air purification
Photocatalysis
Visible-light
Light hydrocarbons

ABSTRACT

Chromium-incorporating mesoporous material denoted as Cr-TUD-1 was synthesized by using a surfactant-free one-pot synthesis procedure. Samples with different chromium loading were prepared and extensively characterized by means of X-ray diffraction (XRD), UV–vis and Raman spectroscopy, X-ray photoelectron spectroscopy (XPS), $^{29}$Si MAS NMR, high-resolution transition electron microscopy (HR-TEM), nitrogen physisorption and elemental analysis. Characterization results show that as a function of Cr loading, Cr exists in different morphological structures such as isolated tetrahedrally coordinated $Cr^{6+}$, nano-particulates, and finally bulky crystalline $Cr_2O_3$. The catalytic performance of the Cr-TUD-1 samples was investigated in the gas phase photo-catalytic oxidation of a mixture of light hydrocarbons i.e. methane, ethylene, ethane, propylene, and propane by molecular oxygen. Isolated $Cr^{6+}$ species were found to be more active than $Cr^{3+}$. The sample with 5 wt.% Cr loading which contains a mixture of $Cr^{6+}$ and $Cr^{3+}$ moieties was found to be the most active sample. A mechanism is proposed to show the synergy between $Cr^{6+}$ and $Cr^{3+}$. Cr-TUD-1 was found to be stable under dry conditions, the photocatalytic oxidation rates of the different hydrocarbons were almost the same up to six runs, however, the presence of water vapour in the reaction mixture causes serious deactivation to the catalyst. The activity of Cr-TUD-1 was superior to other metals-incorporated TUD-1 (e.g. Ti, V, and Mo) or other Cr-containing mesoporous materials (e.g. Cr-MCM-41 and Cr–$SiO_2$) under the same reaction conditions.



## 1. Introduction

Release of volatile short-chain hydrocarbons may occur during their use in different chemical industrial processes. They are produced from combustion processes, such as waste incineration. Furthermore, they are found in vehicle exhaust fumes as well as the combustion of natural gas in gas power plants [1–3]. Short chain hydrocarbons are considered to be air pollutants with a considerable contribution in the global warming because of their high potential as greenhouse gases [4,5]. Moreover, they have a negative effect on human lungs and might cause damage to the central nervous system upon prolonged exposures. Methane has the highest potential in the global warming (21 times higher than carbon dioxide) ranks it amongst the worst of the greenhouse gases [6]. Super-saturation environment of ethane has serious risk of suffocation [7]. Exposure to high levels of ethylene and propylene can harm wildlife, furthermore, they can be involved in reactions that produce ground level ozone, which can damage crops and materials. Propane is a harmful gas to living organisms, it is harmful to the body if liquid propane comes in contact with skin [7]. Hence, the elimination of short chain hydrocarbon in air became crucial.

Generally speaking, the saturated, short-chain hydrocarbons (e.g. methane, ethane, and propane) are stable and less reactive than the unsaturated alkenes (e.g. ethylene and propylene) because of their inert C—H bonds, which makes their oxidation is difficult and energy consumer process [8–10].

Several attempts have been reported to convert volatile hydrocarbons to carbon dioxide (i.e. complete oxidation process) by using Noble metals (Pt, Pd, Au, Rh) [11–13] as conventional heterogeneous catalysts, other attempts were reported to use transition metal oxides and doped oxides [14,15]. However, the low reactivity and the catalysts poisoning in addition to the required temperature (up to 800 K) have limited their use. Photocatalytic oxidation of short chain hydrocarbons can offer a smart alternative for the

* Corresponding author at: Chemistry Department, Faculty of Science, King Khalid University, P.O. Box 9004, Abha 61413, Saudi Arabia. Tel.: +966 172418892; fax: +966 172417637.
*E-mail address:* m.s.hamdy@gmail.com (M.S. Hamdy).

http://dx.doi.org/10.1016/j.apcatb.2015.03.030
0926-3373/

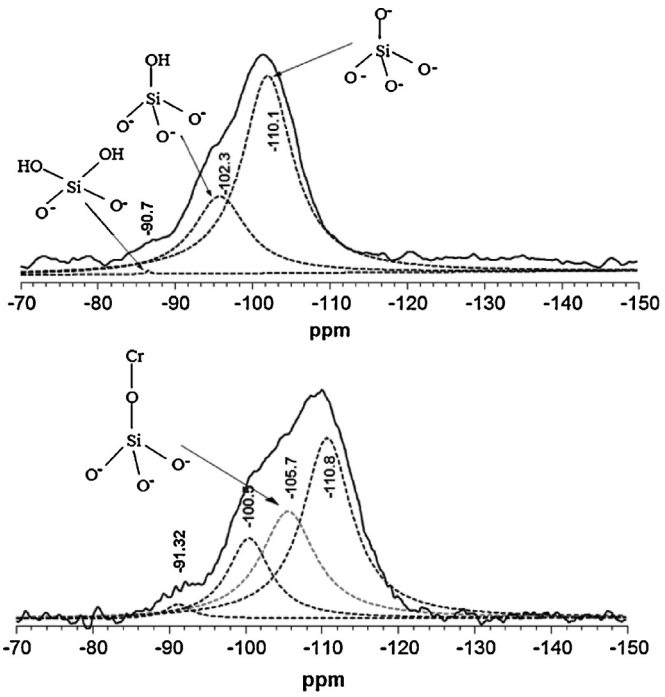


**Fig. 1.** A comparison between $^{29}$Si MAS NMR spectra of TUD-1 sample (top panel) and Cr-TUD-1 (bottom panel).

conventional oxidation process, in which, the oxidation carries out at ambient conditions (temperature and pressure).

The designing of a cost-effective, visible-light sensitive, noble-metal-free material could be additional advantages to create an environmental-friendly photocatalyst. Cr containing different micro-/mesoporous such as Cr-SBA-15, [16] Cr-MCM-48 [17] and Cr-HMS [18], were reported as visible-light sensitive photocatalysts in several applications including short-chain hydrocarbon oxidation. Previously, we presented the three dimensional mesoporous Cr-TUD-1 as a photocatalyst for the selective oxidation of propane to acetone [19,20] to investigate the intermediates formation as a part of the entire photocatalytic oxidation process which normally ends with the formation of $CO_2$ and $H_2O$ as final products.

In the current study, we expanded our previous investigations about Cr-TUD-1, here, Cr-TUD-1 material with different Cr loading was prepared to create different Cr sites. The photocatalytic performance of Cr-TUD-1 in the oxidation of a mixture of short-chain hydrocarbons (methane, ethane, ethylene, propane and propylene) by oxygen is presented. The photocatalytic oxidation rate of the different hydrocarbons is discussed on the basis of the active sites' nature of the photocatalysts. In addition, effect of the presence of water vapour on the photocatalytic rates and the stability of photocatalysts are evaluated.

## 2. Experimental

### 2.1. Catalysts syntheses

Cr-TUD-1 mesoporous materials with different Si/Cr ratios have been synthesized by aging, drying and calcining a homogeneous synthesis mixture, consisting of a solution of chromium nitrate nonahydrate ($Cr(NO_3)_3{\cdot}9H_2O$), tetraethylorthosilicate (TEOS) as a silicon alkoxide source and triethanolamine (TEA) as a bi-functional template. The four synthesized samples donated as Cr-*x*, where *x* is the loading of Cr in the synthesis mixture, i.e. *x* = 1, 2.5, 5, and 10. In a typical synthesis example, for Cr-1, a mixture of 14.4 g of TEA (97%, ACROS) + 3.6 mL of $H_2O$ was added dropwise to TEOS (19.91 g, +98%, ACROS) while stirring. After stirring for about 0.5 h, an aqueous chromium salt solution (0.38 g of chromium nitrate + 2 mL of $H_2O$) was added dropwise to the above mixture, followed by the addition of 19.7 g of tetraethyl ammonium hydroxide (TEAOH, 35%, Aldrich). Finally, a green, clear synthesis mixture was obtained with a molar ratio composition of $SiO_2$ : *x* $Cr_2O_3$ : 0.5 TEAOH : 1 TEA : 11 $H_2O$. The mixture was aged at room temperature for 24 h, dried at 373 K for 24 h, heated in an autoclave at 451 K for 8 h, and then calcined at 873 K for 10 h using a heating ramp rate of 1 K/min in air.

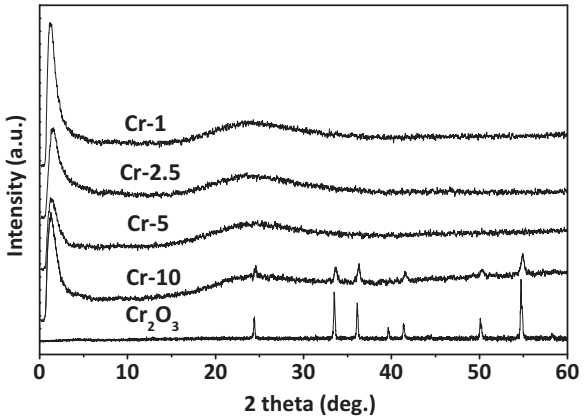


**Fig. 2.** XRD patterns of the different Cr-TUD-1 samples compared with the pattern of $Cr_2O_3$.

For comparison, samples of different metal (i.e. 5 wt.% of Ti, V, and Mo) incorporated TUD-1 were synthetized by following the same synthesis procedure. The prepared samples were detonated as Ti-5, V-5, and Mo-5, respectively.

### 2.2. Characterizations

The prepared samples were characterized by means instrumental neutron activation analysis (INAA), nitrogen phsyisorption, powder X-ray diffraction (XRD), UV–vis spectroscopy, Raman spectroscopy (under ambient and under in-situ heating), $^{29}$Si nuclear magnetic resonance (NMR), high-resolution transmission electron microscopy (HR-TEM) and X-ray photoelectron spectroscopy (XPS). Detailed characterization procedures can be found in the Supporting information section.

### 2.3. Catalytic performance study

The photocatalytic oxidation of hydrocarbons over Cr-TUD-1 was evaluated in a multi-cell home-made photocatalytic set-up [21]. The set-up consists of 12 cylindrical reactors (inner volume 50 mL), which are connected by a sample loop for gas dosage and sampling. The applied light source is a 120 W high-pressure mercury lamp with a spectrum ranging from 280 to 650 nm. All the reactors were operated in batch mode and illuminated for 135 min. The concentration of hydrocarbons was monitored by a compact gas chromatograph equipped with TCD and FID detectors with an accuracy of ±0.5 ppm. Molsieve 5A (5 m) and a capillary Porabond Q column (10 m) were connected to the TCD detector while Porabond Q column (10 m) was connected to the FID detector. A standard gas mixture of 1 vol.% of $CH_4$, $C_2H_4$, $C_2H_6$, $C_3H_6$, and $C_3H_8$ in helium was used as initial reactants. In a real reaction, 150 mg of the catalysts were spread flatly at the bottom of the reactor to make a uniform film with a thickness of 1–2 mm. The reactors were evacuated down to 3 mbar and then a He stream containing 25 ppm of each component was introduced into the reactors over the catalyst films. Evacuation/filling cycle was also repeated at least three times before lamp ignition and starting the degradation experiment.

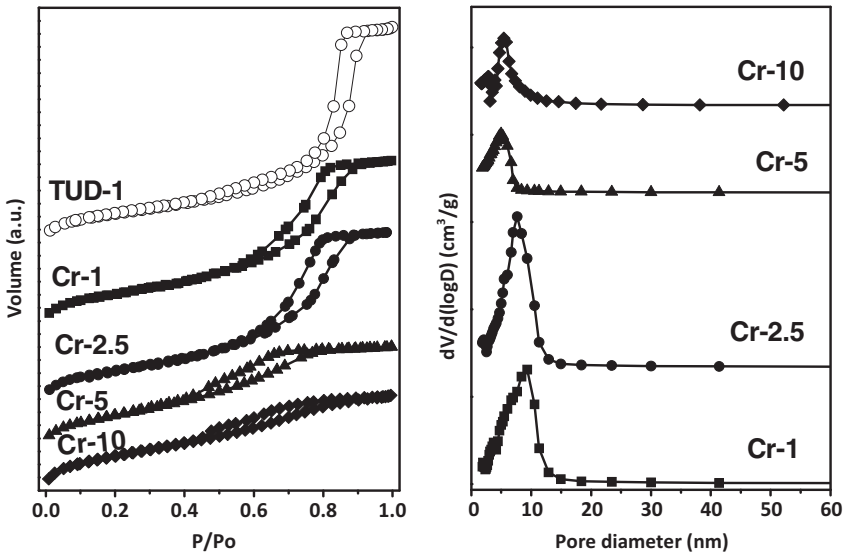


**Fig. 3.** Left panel: $N_2$ isotherms of the different Cr-TUD-1 samples. Right panel: the corresponding pore size distribution.

The photoactivity profiles were fitted assuming first order kinetics:

$$C_M = C_{Mo}\ e^{-kt}$$

where $C_M$ is the concentration of the hydrocarbons at time $t$, $C_{Mo}$ is the initial concentration, and $k$ is the observed rate constant.

The effect of water was studied exactly as described earlier, with one exception, 4 vol.% of water vapour was introduced with the feed of gases into the reactors. The stability and reusability test was carried out for Cr-5 sample. In this test, the gases were evacuated from the reactor after the first run, and then fresh gases mixture was introduced for the second run and so on. This process has been repeated six times without any treatment for the catalyst. All the experiments were carried out at least for three times, the results presented here is the average of the three with a standard deviation does not exceed than 3%.

## 3. Results

### 3.1. The morphology of the samples

$^{29}$Si MAS NMR was performed to study the interaction between Si and Cr in the Cr-TUD-1 sample. The $^{29}$Si MAS NMR spectrum of the calcined siliceous TUD-1 sample is compared with the Cr-5 spectrum in Fig. 1. The spectrum of siliceous TUD-1 was deconvoluted into three peaks, the first around −110 ppm which is usually assigned to (—O—)$_4$Si with no OH group attached to the silicon atom ($Q_4$). The second peak appearing around −102 ppm is assigned to (—O—)$_3$Si(OH) with one OH group ($Q_3$). The last peak around −90 ppm, is assigned to (—O—)$_2$Si(OH)$_2$ with two OH groups ($Q_2$). These peaks were also detected in spectrum of the Cr-5 sample, albeit with a shift of the −102 ppm peak to −100.5 ppm. Moreover, an additional peak is observed at −105.7 ppm, which might be attributed to the mentioned interaction of Si with Cr incorporated in the TUD-1 framework [(—O—)$_3$Si—O—Cr] [22,23].

Fig. 2 shows the powder XRD patterns of various samples of Cr-TUD-1 compared with $Cr_2O_3$. All samples show a single intensive peak at 0.1–2.5° 2$\theta$, indicating that Cr-TUD-1 is a meso-structured material. In addition, the powder XRD patterns of Cr-1, Cr-2.5, and Cr-5 show no detectable $Cr_2O_3$ phase or other crystalline chromia species. However, Cr-10, with a high Cr-loading (Si/Cr ratio = 10) shows additional peaks around 25, 36, 38, 42, and 55° 2$\theta$, which are consistent with the presence of a $Cr_2O_3$ phase in Cr-10. The formation of crystalline $Cr_2O_3$ in the Cr high-loaded mesoporous materials was also observed in Cr-SBA-15 and Cr-MCM-41 [24,25].

The elemental analysis of the different Cr-TUD-1 samples is summarized in Table 1. Comparing the composition of the synthesis gel and that of the obtained powder after calcination, indicates that almost all the metal added during synthesis ends up in the final solid product. In Table 1, the porosity measurements of the Cr-TUD-1 samples (calculated from the adsorption branch of an $N_2$ adsorption–desorption isotherms using the Barrett–Joyner–Halenda formula) are summarised: the surface area of the samples increased with Cr-loading from 565 to 634 m$^2$/g, the pore volume ranged from 1.1 to 1.7 cm$^3$/g and the mesopore diameter ranged from 4.4 to 9.1 nm. The high surface area of Cr-10 sample is presumably the consequence of the introduction of micropores of Cr-oxide crystals.

The $N_2$ adsorption/desorption isotherms of the calcined Cr-TUD-1 samples are compared with the mesoporous siliceous TUD-1 sample in Fig. 3, left panel. All the isotherms showed type IV isotherms, representative for mesoporous materials according to IUPAC classification. Moreover, two different types of hysteresis loops can be distinguished, in the loops of Cr-1 and Cr-2.5, the loops are relatively narrow, the adsorption and desorption branches being almost vertical and nearly parallel (H1), which means that the pore system is uniform, cylindrical and no interconnectivity could be observed. While in Cr-5 and Cr-10, the hysteresis loops become broad, the desorption branch being much steeper than the adsorption one, and the pore filling and emptying profile indicates the presence of a wide range of non-uniform pores (H3). This behaviour is normally observed in the partially blocked mesopors which can be explained by the formation of chromium oxide nanoparticles inside the mesopores of TUD-1. The surface area of Cr-1 is smaller than the parent TUD-1 sample, however, it increases as a function of increasing chromium loading. At the same time, the mesopore diameter and the mesopore volume decrease (Fig. 3, right panel), which is consistent with the formation of chromium oxide crystals in the samples of high Mo-loading. Similar trends were also reported for Fe-TUD-1 [26] and Mo-TUD-1 [27].

The mesoporous and amorphous structure of the samples was further confirmed by HR-TEM (Fig. 4). The micrograph of the Cr-1 sample shows the irregular sponge-like characteristics of TUD-1, no crystalline phase(s) could be observed, which means that all the Cr atoms are incorporated in the framework of TUD-1. In the

**Table 1**
The texture properties of the different Cr-TUD-1 samples as obtained from elemental analysis and $N_2$ sorption measurements.

| Sample | Colour[a] | | Si/Cr ratio | | $S_{BET}$[b] ($m^2/g$) | $V_{meso}$[c] ($cm^3/g$) | $D_{meso}$[d] (nm) |
|---|---|---|---|---|---|---|---|
| | Uncalcined | Calcined | Synthesis mixture | Calcined | | | |
| TUD-1 | Brown | White | ∞ | ∞ | 655 | 0.7 | 4.5 |
| Cr-1 | Light green | Yellow | 100 | 130 | 565 | 1.54 | 8.4 |
| Cr-2.5 | Light green | Orange | 40 | 40.3 | 572 | 1.70 | 7.4 |
| Cr-5 | Light green | Dark orange | 20 | 18.2 | 588 | 1.09 | 4.4 |
| Cr-10 | Dark green | Green | 10 | 9.98 | 634 | 1.14 | 9.1 |

[a] A picture illustrating the colour of the prepared Cr-TUD-1 samples is presented in Supplementary information section, Fig. S1.
[b] Specific surface area.
[c] Mesopore volume.
[d] Mesopore diameter.

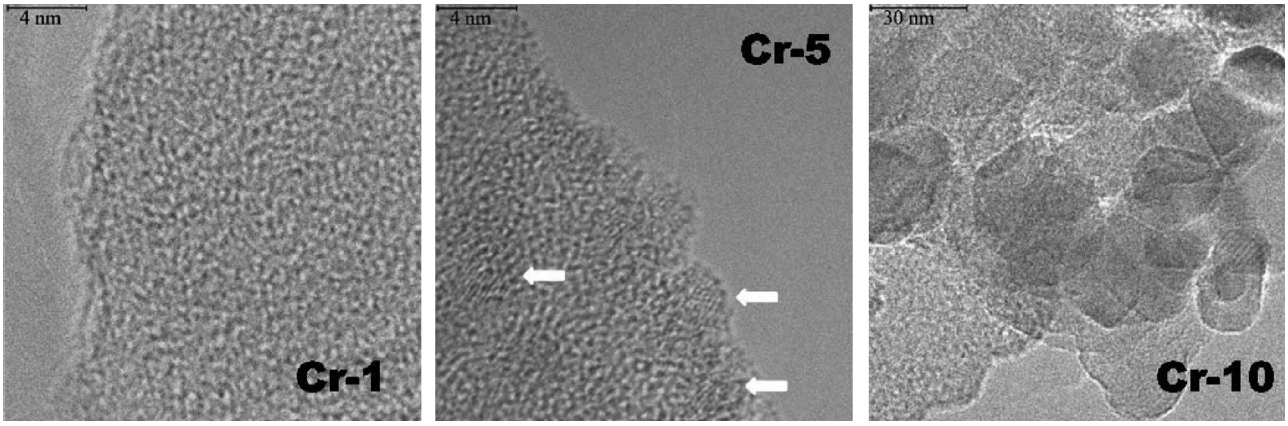


**Fig. 4.** HR-TEM micrographs of Cr-1 (left panel), Cr-5 (middle panel) and Cr-10 (right panel).

micrograph of Cr-5 sample, few nano-particles (in the range of 2–4 nm) of Cr oxide could be detected. Furthermore, no bulky crystalline Cr oxide could be detected. Finally, in Cr-10 the HR-TEM micrograph shows extra-framework crystalline $Cr_2O_3$, with particle sizes of 100–200 nm.

The UV–vis spectra of the calcined Cr-TUD-1 samples are shown in Fig. 5. The spectra are dominated by: two intense bands around 270 and 350 nm, a shoulder around 440 nm and a weak band around 600 nm are observed only in high Cr-loading samples. The adsorption bands centred at 270 and 350 nm are usually assigned to the charge transfer from $O^{2-}$ to $Cr^{6+}$ of the tetrahedrally coordinated $Cr^{6+}$ and indicate the presence of highly isolated $Cr^{6+}$ atoms inside the silica matrix [28,29]. The shoulder around 440 nm is characteristic of $Cr^{6+}$ polychromate (—Cr—O—Cr—)*n* in the framework.

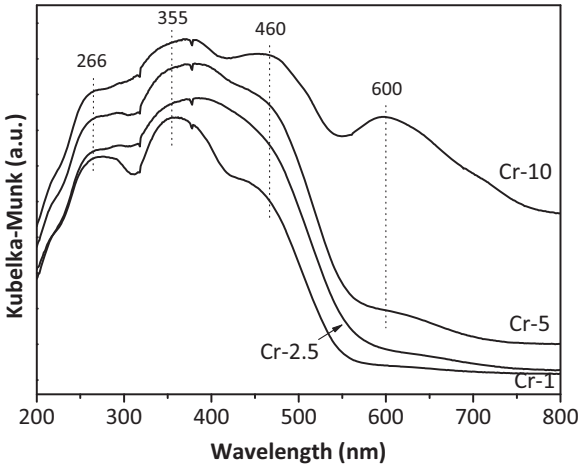


**Fig. 5.** UV–vis spectra of Cr-TUD-1, the spectra collected at ambient conditions.

Additionally, the peak around 600 nm is typically associated with the presence of octahedral $Cr^{3+}$ consistent with the presence of extra-framework $Cr_2O_3$ clusters.

Raman spectra of Cr-TUD-1 samples were collected at ambient condition (Fig. 6 left panel) and under dehydration conditions (Fig. 6, right panel). Under ambient conditions, the spectra of Cr-1, Cr-2.5 and Cr-10 samples are dominated by a Raman band at 897 $cm^{-1}$. This peak is attributed by monohromate species of $Cr^{6+}$ state [30]. In Cr-5 spectrum, two additional bands were observed, the first band at 975 $cm^{-1}$ can be attributed to the polychromate $Cr^{6+}$ species [31]. The second band at 550 $cm^{-1}$ is attributed to the octahedral $Cr^{3+}$ in crystalline phase of $Cr_2O_3$ [32].

Under dehydration conditions, the in-situ Raman spectra of Cr-1, Cr-2.5 and Cr-5 samples are dominated by a band at 980 $cm^{-1}$ which is decreasing with the Cr loading. It was reported by Wachs and co-workers [33,34] that this band is attributed to the presence of di-oxo chromate species $(Si—O)_2Cr(=O)_2$. Moreover, a very small shoulder was also observed at 1012 $cm^{-1}$ (clearly visible in Cr-2.5 spectrum), this shoulder was described to be attributed to the presence of monoxo chromate species $(Si—O)_3Cr(=O)$. The bands between 325 and 400 $cm^{-1}$ are attributed to the O—Cr—O bending modes [33,34].

Fig. 7 shows the X-ray photoelectron spectroscopic peaks for Cr-TUD-1 samples as compared to $Cr_2O_3$ and $CrO_3$ as references. The Cr-1 sample did not show any peaks (not presented in the figure). This is most probably due to the low surface loading. For all of the samples (except in Cr-1), the two peaks (Cr $2p_{3/2}$ and Cr $2p_{1/2}$) could be decomposed into a peak located at a value of about 577.5 ± 0.5 eV attributed to trivalent Cr [35] and a value of about 580.7 ± 0.5 eV for hexavalent Cr [36]. It was observed that the colour of the sample changed from shade of brown to a shade of green during the recording of the photoelectron spectra of the chromium containing catalysts. This may be due to a photo reduction under the X-ray beam of hexavalent chromium oxide to trivalent chromium

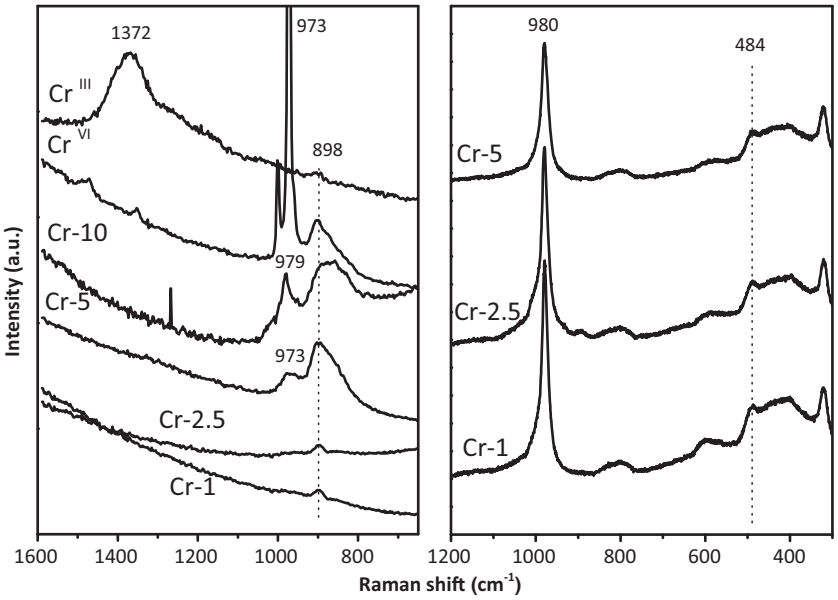


**Fig. 6.** Raman spectra of Cr-TUD-1 samples, spectra collected at ambient conditions (left panel) and under dehydration conditions (right panel).

oxide and hence the Cr-10 sample seemed to contain only trivalent chromium. XPS study clearly indicates that at lower Cr loading (up to 5% loading) Cr atoms are mainly in hexavalent coordination state. While at high Cr content, (i.e. Cr-10) Cr atoms are mainly in trivalent state. These results are in agreement with other characterization data as well as other literature [37–40]. Based on the obtained characterization data, it is clear that different Cr sites can be generated by changing the Cr loading during the synthesis.

### 3.2. The photocatalytic performance

#### 3.2.1. Loading effect

Fig. 8 shows the first order rate constant ($k$) of the photocatalytic degradation of the different applied gases over Cr-TUD-1 samples compared with siliceous TUD-1, $CrO_3$ and $Cr_2O_3$. Cr-5 exhibited an extra-ordinary photocatalytic activity in oxidation of propylene, ethylene and propane. Small conversion of ethane was obtained, while methane showed high stability at room temperature. The oxidation rate of the applied hydrocarbons was in the following order: Propylene » propane >= ethylene > ethane. The degradation profiles can be found in Supplementary information, Fig. S2.

To investigate the role of oxygen in the oxidation process, a control reaction was carried out without oxygen, i.e. only hydrocarbons mixture over the Cr-5 sample with light, very minor conversion was obtained (Fig. S3). This indicates the needs of atomic oxygen to perform the photocatalytic reaction.

#### 3.2.2. Comparison with other $MO_x$-TUD-1

The comparison between the photocatalytic activities of different metal-incorporated TUD-1 (metal = Cr, Mo, V and Ti) with the same metal loading (5 wt.%) is presented in Fig. 9.

Based on our previous studies [27,40], the four samples contain nanoparticles of metal oxides incorporated in TUD-1 silica matrix. It is clear that Cr-5 is the most active photocatalyst in the oxidation of C1–C3 hydrocarbons. Mo-5 exhibited considerable activity, however it is much less than Cr-5. Moreover, the oxidation rate of the different hydrocarbons showed a little different order than Cr-5. In Cr-5 the order was propylene > propane >= ethylene > ethane, the same order was also observed in Cr-1, however, in Mo-5 the order of the degradation rates was propylene > ethylene > propane,

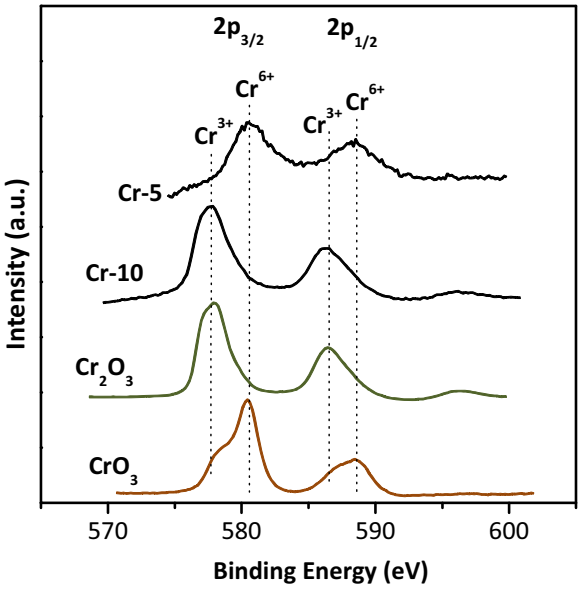


**Fig. 7.** XPS spectra Cr-TUD-1 samples compared with $CrO_3$ and $Cr_2O_3$.

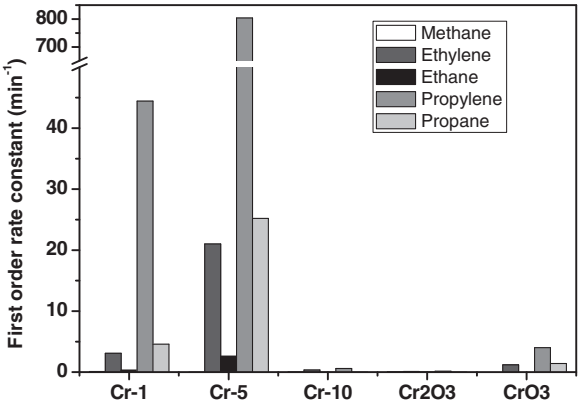


**Fig. 8.** First order rate constant of the C1–C3 photocatalytic degradation over different Cr-TUD-1 samples as compared with Cr-oxides references.

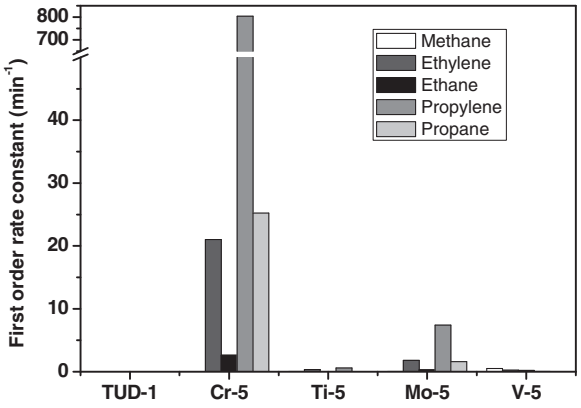


**Fig. 9.** First order rate constant of the C1–C3 photocatalytic degradation over different metals incorporated TUD-1.

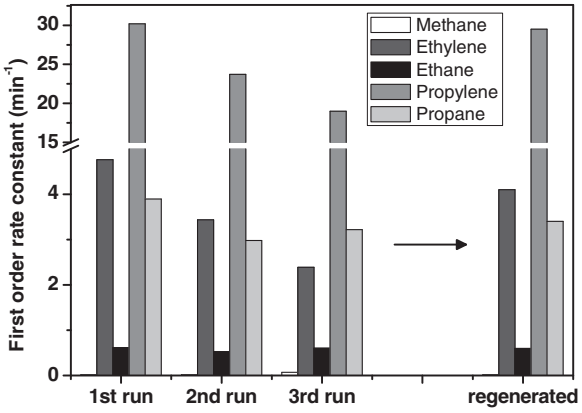


**Fig. 11.** Recycling of Cr-5 sample under hydrated conditions, the sample was reused for three runs without treatment and the 4th run was after regeneration by heat.

while ethane and methane seem to be stable over Mo-5 and did not oxidized. The photocatalytic activities of V-5 and Ti-5 are absolutely negligible. The poor activity of Ti-5 is in agreement with our previous study of propane oxidation over $TiO_2$-TUD-1 in which the photocatalytic activity of low loading of $TiO_2$ nanoparticles supported on silica is considered to be negligible if the loading was <40 wt.% [40].

### 3.2.3. Effect of water vapour

To explore the relationship between the photocatalytic activity of Cr-5 and the humidity, another control reaction was carried out and water vapour was fed with the gases into the reactor. A comparison between the photocatalytic activity of Cr-5 when the feeding gases were dry and wet is presented in Fig. 10. When water vapour added to the feed in excess amount (i.e. 4 vol.%), the photocatalytic activity of Cr-5 was found to be decreased sharply, which means that water vapour has a negative effect on the overall photocatalytic process.

### 3.2.4. Stability and reusability

Cr-5 sample exhibited a good stability under dry conditions, i.e. when the feed mixture was water-free. The photocatalytic oxidation reaction of the hydrocarbons was repeated over the same sample for continuous six times, the same oxidation rates for the different applied hydrocarbons were obtained. After the sixth run, the photocatalytic activity of the samples was decreased gradually due to the accumulation of the oxidation process products, notably water. The sample in the end of the 10th run, tended to gain a pale green colour to become greenish-orange (see Fig. S4 in the Supporting information section) and the catalyst lost more than 45% of its activity, this is most likely due to reduction of $Cr^{6+}$ to $Cr^{3+}$.

Under wet conditions (Fig. 11), the photocatalytic activity of Cr-5 sample showed serious deactivation from one run to another. After the 3rd run, Cr-5 sample almost lost 20–25% of its activity, and the sample gained the greenish colour as an indication for the reduction of $Cr^{6+}$ to $Cr^{3+}$. When the used sample under wet conditions heated for 673 K for 4 h under autogenous conditions, the sample retained its original activity once more, due to the removal of contaminations and water molecules accumulated on the surface of the sample, and hence the active sites were set free and clean. More importantly, by heating the sample, the greenish colour disappeared, and the sample became bright orange again. Similar deactivation–reactivation behaviour was reported by Sun et al. [41].

### 3.2.5. The effect of the support

As a final note, the photocatalytic performance of Cr-TUD-1 (Cr-1 sample) was compared with 1% Cr supported on MCM-41 mesoporous material and with commercial $SiO_2$ (Fig. 12). Under the same reaction conditions, Cr-TUD-1 showed a significantly better activity than Cr–$SiO_2$ (almost six to seven times higher) and Cr-MCM-41 (almost two to three times higher). This can be explained by three dimensional open structure of TUD-1 which offers high accessibility towards the Cr sites.

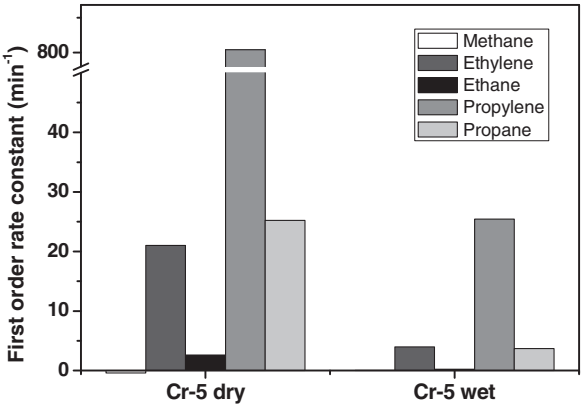


**Fig. 10.** The effect of water on the photocatalytic activity of Cr-TUD-1 in the degradation of C1–C3 hydrocarbons.

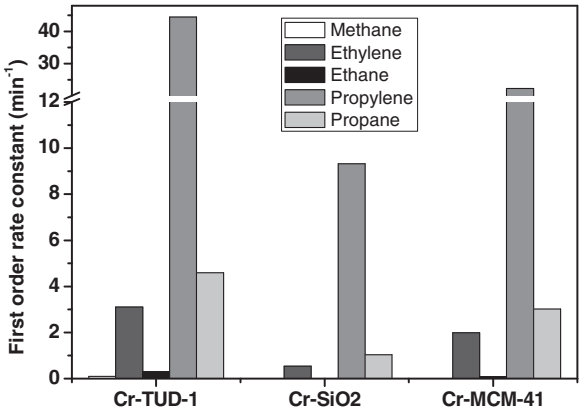


**Fig. 12.** First order rate constant of the C1–C3 photocatalytic oxidation over 1 wt.% Cr supported on TUD-1, $SiO_2$, and MCM-41.

$$Cr^{6+}—O^{2-} \xrightarrow{h\nu} [Cr^{5+}—O^{-}]^{*} \quad (1)$$

$$C_nH_{2n+2} \xrightarrow[C_nH_{2n}]{O_2} [Cr^{5+}—O^{-}]^{*} \xrightarrow{\text{Over oxidation}} [\text{Intermediates}] \xrightarrow[O_2]{} [Cr^{5+}—O^{-}]^{*} \rightarrow CO_2 + H_2O \quad (2)$$

**Scheme 1.** The photocatalytic oxidation of the hydrocarbons.

## 4. Discussions

During the synthesis of Cr-TUD-1, it is obviously clear that different active sites can be obtained by varying the amount of Cr in the synthesis mixture. Cr-1 contained only one type of active sites, i.e. $Cr^{6+}$ isolated species with two oxo-bridges, Cr-5 contains majority of $Cr^{6+}$ in the form of isolated sites, polychromate and/or nanoparticles of $CrO_3$, in addition to a minority of $Cr^{3+}$ moieties, while Cr-10 contains a majority of $Cr^{3+}$ in the form of extra framework $Cr_2O_3$ bulky crystals. Synthesis of different Cr active sites (from isolated to bulky oxide crystals) supported on different mesoporous materials was reported by Selaraj et al. when SBA-15 was used as a support and by Yamashita et al. when HMS mesoporous material was used as a support [42,43].

In Cr-1 sample, where the majority of the Cr species are $Cr^{6+}$ with dioxo-bridges, upon illumination in the visible light region, a charge transfer from $O^{2-}$ to $Cr^{6+}$ yields $(Cr^{5+}–O^{-1})^{*}$, and the reactive oxygen atom initiates chemistry with adsorbed hydrocarbon molecules which undergoes a series of consecutive oxidation reactions to produce $CO_2$ and $H_2O$ as final products (Scheme 1). Hence, the obtained photocatalytic performance of Cr-1 is in a total agreement with the previous reports [42,43].

The superior activity of Cr-5 must be explained by the co-presence of $Cr^{6+}$ and $Cr^{3+}$ species since the difference in activity between Cr-1 and Cr-5 is not quantitatively feasible, i.e. the recorded activity of Cr-5 is not 5 times higher than that of Cr-1. Furthermore, as mentioned previously, the characterization data confirmed the co-existence of a majority of $Cr^{6+}$ (in the form of $CrO_3$ nanoparticles, isolated $Cr^{6+}$ sites and polychromate $Cr^{6+}$) and a minority of $Cr^{3+}$ moieties in TUD-1 matrix. The applied lamp covers a wide range of wavelength, hence, both types of Cr—O moieties can absorb photons and generate electron/hole pairs (see Fig. S5 in Supplementary information). A possible mechanism is proposed in Fig. 13, in which electron/hole pairs will be formed on both moieties, the holes formed on $Cr^{3+}$ moieties will work as a trap for the electron formed on $Cr^{6+}$ moieties if the electrons can reach the holes level, which is very possible because the energy difference between the conduction band of $Cr^{6+}$ and the valence band of $Cr^{3+}$ is very small i.e. approximately 0.25 eV [44]. Based on the proposed mechanism the electron/hole separation is increased and hence more reactions will take place. The role of $Cr^{3+}$ in the proposed mechanism is very similar that proposed by Zhu et al. [45], Irie et al. [46] and Fan et al. [47] in the explanation of the high activity of $TiO_2$ graphed with $Cr^{3+}$ moieties. The high activity of the supported chromia catalysts which contains a majority of $Cr^{6+}$ and minority of $Cr^{3+}$ was observed by Elías et al. [25] and by Wang et al. [30]; however, the reports did not introduce a possible explanation.

The many differences between the Cr-5 and bulky crystalline $CrO_3$ can explain the great difference in the photocatalytic performance between the two samples. Generally speaking, the factors of the absence of $Cr^{3+}$–$Cr^{6+}$ synergy, particle size, surface area, active sites distribution, and the role of the support draw the main differences between the two samples. The particle size of $CrO_3$ nano-particles supported on TUD-1 is much smaller than the bulky

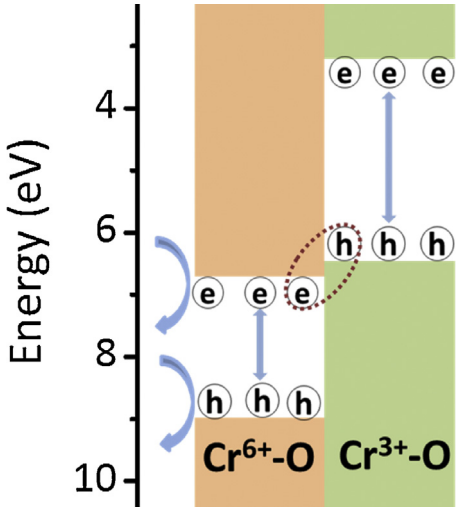


**Fig. 13.** Scheme of the proposed electron and hole transfer processes between the nanoparticles of $Cr^{6+}$ and $Cr^{3+}$ explaining the high photocatalytic activity of the Cr-5 sample.

crystals, i.e. 2–4 nm vs. 40 μm, respectively. This will lead to the second difference, the high surface area of Cr-5 sample (i.e. 580 $m^2/g$) nanoparticles vs. the small surface of the bulky $CrO_3$ (6 $m^2/g$). Moreover, the high dispersion of the $CrO_3$ nanoparticles in the 3D open-structural, of TUD-1 offers an excellent accessibility to/from the active sites; however, in bulky $CrO_3$, only the surface active sites will be available for the reaction. Furthermore, it has been reported that the mesoporous material could act as a "sponge" [48,49] and the mesoporous material could pre-concentrate the substrate, making it available for the $CrO_3$ nano-particles to perform the photocatalysis. The poor activity of Cr-10 is expected, and it can be explained by the presence of majority $Cr^{3+}$ as bulky crystalline $Cr_2O_3$ which has been reported that is it not photocatalytically active due to the partially filled *d* orbital [50]. Furthermore, the presence of those bulky crystals shields/prevents the light to reach the small quantity of $Cr^{6+}$ species present in the silica matrix. To the best of our knowledge, $Cr_2O_3$ as individual material did not report before as a photocatalyst, which is in agreement with our finding.

## 5. Conclusions

In the present study, Cr-TUD-1 showed a high activity in the degradation of five different mixed hydrocarbon gases. The sample contains $Cr^{6+}$ and $Cr^{3+}$ moieties exhibited a superior photocatalytic activity than the sample which contains only $Cr^{6+}$ moieties. A possible scenario about the synergy between $Cr^{6+}$ and $Cr^{3+}$ is proposed to explain such high activity. The degradation rate of the gases was in the order of propylene » ethylene >= propane > ethane while very low degradation of methane was observed. Cr-TUD-1 was highly stable under dry conditions, however, it was influenced by the presence of water vapour and it deactivated rapidly. The

photocatalytic activity of Cr-TUD-1 benchmarked the other metal oxides nanoparticles containing TUD-1 (e.g. $TiO_2$, $V_2O_5$, and $Mo_2O_3$) and Cr containing other supports such as $SiO_2$ and MCM-41.

## Acknowledgements

The authors thank Dr. P.J. Kooyman, TU Delft, The Netherlands, for the HR-TEM micrographs and Dr. J. Groen for the $N_2$ sorption measurements. Dr. S. Choi, and Dr. I.E. Wachs, Lehigh University, USA, are greatly acknowledged for assistance in recording and interpretation of the in situ Raman measurements under dehydrated conditions.

## Appendix A. Supplementary data

Supplementary data associated with this article can be found, in the online version, at http://dx.doi.org/10.1016/j.apcatb.2015.03.030.

## References

[1] R.P. Pohanish, Sittig's Handbook of Toxic and Hazardous Chemicals and Carcinogens, William Andrews Publishing, New York, 2002.
[2] P.R. Gogate, A.B. Pandit, Adv. Environ. Res. 8 (2004) 501.
[3] T.V. Choudhary, S. Banerjee, V.R. Choudhary, Appl. Catal. A 234 (2002) 1.
[4] EPA, Total exposure assessment methodology (TEAM) study, in: Report 600/6–87/002a, Environmental Protection Agency, Washington, DC, 1987.
[5] US EPA, National Emission Standards for Hazardous Air Pollutants, 40 CFR, part 63, (2006).
[6] A.R. Moss, J.-P. Jouany, J. Newbod, Ann. Zootech. 49 (2000) 231.
[7] Handbook of Compressed Gases, Springer, 4th ed., (1999), pp. 348.
[8] M.A. Banares, Catal. Today 51 (1999) 319.
[9] Y. Boutadla, D.L. Davies, S.A. Macgregor, A.I. Poblador-Bahamonde, Dalton Trans. 30 (2009) 5820.
[10] N. Kuhl, M.N. Hopkinson, J. Wencel-Delord, F. Glorius, Angew. Chem. Int. Ed. 51 (2012) 10236.
[11] R.F. Hicks, H. Qi, M.L. Young, R.G. Lee, J. Catal. 122 (1990) 280.
[12] M. Aryafar, F. Zaera, Catal. Lett. 48 (1997) 173.
[13] A.C. Gluhoi, N. Bogdachikova, B.E. Nieuwenhuys, Catal. Today 113 (2006) 178.
[14] M.C. Marion, E. Garbowski, M. Primet, J. Chem. Soc. Faraday Trans. 86 (1990) 3027.
[15] V.R. Choudhary, B.S. Upadhe, S.G. Pataskar, A. Keshavraja, Angew. Chem. Int. Ed. 35 (1996) 2393.
[16] L. Zhang, Y. Zhao, H. Dai, H. He, C.T. Au, Catal. Today 131 (2008) 42.
[17] S. Shen, L. Guo, Catal. Today 129 (2007) 414.
[18] H. Yamashita, K. Yoshizawa, M. Ariyuki, S. Higashimoto, M. Che, M. Anpo, Chem. Commun. 5 (2001) 435.
[19] M.S. Hamdy, O. Berg, J.C. Jansen, Th. Maschmeyer, J.A. Moulijn, G. Mul, Catal. Today 117 (2006) 337.
[20] O. Berg, M.S. Hamdy, Th. Maschmeyer, J.A. Moulijn, M. Bonn, G. Mul, J. Phys. Chem. C 112 (2008) 5471.
[21] C.-C. Yang, J. Vernimmen, V. Meynen, P. Cool, G. Mul, J. Catal. 284 (2011) 1.
[22] P.H.K. Charan, G.R. Rao, J. Porous Mater. 20 (2013) 81.
[23] M. Magi, E. Lippmaa, A. Samoson, G. Engelhardt, A.R. Grimmer, J. Phys. Chem. 88 (1984) 1518.
[24] P. Michorczyk, P. Pietrzyk, J. Ogonowski, Micropor. Mesopor. Mater. 161 (2012) 56.
[25] V. Elías, E. Sabre, K. Sapag, S. Casuscelli, G. Eimer, Appl. Catal. A 413–414 (2012) 280.
[26] M.S. Hamdy, G. Mul, J.C. Jansen, A. Ebaid, Z. Shan, A.R. Overweg, Th. Maschmeyer, Catal. Today 100 (2005) 255.
[27] M.S. Hamdy, G. Mul, Catal. Sci. Technol. 2 (2012) 1894.
[28] B.M. Weckhuysen, I.E. Wachs, R.A. Schoonheydt, Chem. Rev. 96 (1996) 3327.
[29] J.S.T. Mambrim, H.O. Pastore, C.U. Davanzo, E.J.S. Vichi, O. Nakamura, H. Vargas, Chem. Mater. 5 (1993) 166.
[30] G. Wang, L. Zhang, J. Deng, H. Dai, H. He, C.T. Au, Appl. Catal. A 355 (2009) 192.
[31] L. Zhang, Y. Zhao, H. Dai, H. He, C.T. Au, Catal. Today 131 (2008) 42.
[32] M.S. Kumar, N. Hammer, M. Ronning, A. Holmen, D. Chen, J.C. Walmsley, G. Oye, J. Catal. 261 (2009) 116.
[33] E.L. Lee, I.E. Wachs, J. Phys. Chem. C 111 (2007) 14410.
[34] H. Tian, C.A. Roberts, I.E. Wachs, J. Phys. Chem. C 114 (2010) 14110.
[35] S. Derossi, G. Ferraris, S. Fremiotti, E. Garrone, G. Ghiotti, M.C. Campa, V. Indovina, J. Catal. 148 (1994) 36.
[36] D.S. Kim, I.E. Wachs, J. Catal. 142 (1993) 166.
[37] A. Hakuli, A. Kytokivi, A.O.I. Krause, Appl. Catal. A 190 (2000) 219.
[38] B. Liu, M. Terano, J. Mol. Catal. A 172 (2001) 227.
[39] A. Hakuli, A. Kytokivi, A.O.I. Krause, T. Suntola, J. Catal. 161 (1996) 393.
[40] M.S. Hamdy, R. Amrollahi, I. Sinev, B. Mei, G. Mul, J. Am. Chem. Soc. 136 (2014) 594.
[41] B. Sun, E.P. Reddy, P.G. Smirniotis, Appl. Catal. B 57 (2005) 139.
[42] M. Selaraj, S. Kawi, Chem. Mater. 19 (2007) 509.
[43] H. Yamashita, M. Anpo, Curr. Opin. Solid State Mater. Sci. 7 (2003) 471.
[44] M.T. Greiner, M.G. Helander, W.M. Tang, Z. Wang, J. Qiu, Z.H. Lu, Nature 11 (2012) 76.
[45] J. Zhu, Z. Deng, F. Chen, J. Zhang, H. Chen, M. Anpo, J. Huang, L. Zhang, Appl. Catal. B 62 (2006) 329.
[46] H. Irie, T. Shibanuma, K. Kamiya, S. Miura, T. Yokoyama, K. Hashimoto, Appl. Catal. B 96 (2010) 142.
[47] X. Fan, X. Chen, S. Zhu, Z. Li, T. Yu, J. Ye, Z. Zou, J. Mol. Catal. A 284 (2008) 155.
[48] C.C. Aquino, H.O. Pastore, A.F. Masters, T. Maschmeyer, ChemCatChem 3 (2011) 1759.
[49] A. Jentys, R.R. Mukti, J.A. Lercher, J. Phys. Chem. B 110 (2006) 17691.
[50] A. Kudo, Y. Miseki, Chem. Soc. Rev. 38 (2009) 253.